Scanning Microscopy

Volume 1 | Number 3 Article 17

6-10-1987

Electron Microprobe Analysis and Proton Induced X-Ray Spectrometry Applied to Trace Element Analysis in Sulfides: Problems and Prospects

G. Remond
Bureau de Recherches Géologiques et Minières

F. Cesbron
Bureau de Recherches Géologiques et Minières

K. Traxel
Physikalisches Institut der Universität Heidelberg

J. L. Campbell
Guelph-Waterloo Program for Graduate Work in Physics

L. J. Cabri
Canada Centre for Mineral and Energy Technology

Scanning Microscopy, Vol. 1, No. 3, 1987 (Pages 1017-1037) 0891-7035/87$3.00+.00
Scanning Microscopy International, Chicago (AMF O'Hare), IL 60666 USA

ELECTRON MICROPROBE ANALYSIS AND PROTON INDUCED X-RAY SPECTROMETRY APPLIED TO TRACE ELEMENT ANALYSIS IN SULFIDES : PROBLEMS AND PROSPECTS

G. Remond[1]*, F. Cesbron[1], K. Traxel[2], J.L. Campbell[3] and L.J. Cabri[4]

(1) Bureau de Recherches Géologiques et Minières - B.P. 6009 - 45060 Orleans Cedex 2, France.
(2) Physikalisches Institut der Universität Heidelberg - D-6900 Heidelberg, FRG.
(3) Guelph-Waterloo Program for Graduate Work in Physics, Guelph, Ontario, Canada, N1G 2W1.
(4) Canada Centre for Mineral and Energy Technology - 555 Booth Street, Ottawa, Ontario, Canada, K1A 0G1.

(Received for publication October 27, 1986, and in revised form June 10, 1987)

Abstract

The complementary techniques of EPMA and micro-PIXE are reviewed in the context of spatially resolved trace element analysis of sulfide minerals. Attention is focussed on methods of standardization and of fitting EDX spectra. Sphalerites and chalcopyrites from various sources are used as specimens. For Ag in chalcopyrites, the two techniques agree well. Sphalerites pose problems such as Zn-Fe replacement and the presence of minor elements, both of which influence matrix corrections ; these are addressed in detail. The necessity for absorbers in the micro-PIXE work prevents detection of minor elements lighter than Zn ; these are determined by EPMA and the results used in the micro-PIXE fitting and matrix corrections. For Cd, Ag, Ga, Ge there is acceptable agreement between the two techniques given uncertainties and constraints on samples, but EPMA results for Hg are notably lower than micro-PIXE results. The improvement in detection limits afforded by micro-PIXE over EPMA in these sulfide minerals ranges from ~3 for Ga, Ge, Hg to 10-30 for Se, Ag, Cd, In ; possible further gains are discussed for both techniques.

KEY WORDS : Electron probe microanalysis, proton induced X-ray spectrometry, trace elements, detection limit, chalcopyrite, sphalerite.

* Address for correspondence :
G. REMOND - B.R.G.M. - Département Analyse - B.P. 6009 - 45060 ORLEANS cedex 2 (France) - Phone n° (33) 38.64.31.24

Introduction

Spatially resolved minor and trace element analysis in sulfides is important from two points of view: - from the crystallo-chemical viewpoint, the knowledge of their localization provides information on the physical and geochemical conditions of formation ; - from the viewpoint of economics, it is necessary to localize the contaminating, and the valuable elements and to obtain an accurate balance of their content within the phases contained in the ore.

Automation allows the use of the electron microprobe analyzer (EPMA) for problems that require a very large number of in-situ point repetitive analyses of minerals (10). A few hundred ppm is the usual accepted level for the limit of detection with EPMA for most trace elements in sulfides. The detection levels estimated from statistics are generally unrealistically low because they only take into account the precision of X-ray intensity measurements. The accuracy of quantitative data may also depend upon changes in the spatial distribution of elements within the analyzed volume. Changes in composition can result in contamination of the surface by species carrying trace elements assumed to be present as a bulk impurity. These changes may be introduced either during mechanical polishing (21) or during electron beam irradiation (23).

Within the past decade, the use of accelerators in nuclear physics has been extended from the nuclear physics arena to analytical applications based on nuclear reactions, Rutherford backscattering spectroscopy (RBS) and proton induced X-ray spectrometry (PIXE) in order to characterize the surface and subsurface of materials. For X-ray spectrometry, the major advantage of proton irradiation over electron bombardment is its lower continuous X-ray intensity (bremsstrahlung) which leads to a higher characteristic peak to continuum intensity ratio than that obtained under electron irradiation and thus to better detection limits for PIXE than for EPMA. Proton microprobes (micro-PIXE) are now available to study micro-regions and their use in mineralogy has been recently reviewed by Blank and Traxel (2). Micro-PIXE analysis of major sulfide ore minerals from various massive-sulfide deposits has been discussed by Harris et al.(11) and Cabri et al. (4) (5). These results demonstrated the potential of combining EPMA and micro-PIXE data in research on the geochemistry of sulfides.

Reproducibility, accuracy and statistical precision of quantitative data must be considered in order to define the minimum limit of detection which can be attained by both techniques. Reproducibility must be verified for different intervals of time between successive measurements. Accuracy is the difference between the experimental data and the most probable value. Accuracy is evaluated from data obtained for various experimental conditions with different techniques (18) (21). This approach aims to validate both data acquisition and reduction procedures. Data obtained by different methods and equipment must be compared. The detection limit is obtained from statistical considerations but such an approach may not be fully justified unless the accuracy is evaluated.

The aim of this paper is to compare the respective analytical efficiencies of EPMA and micro-PIXE. Chalcopyrites and sphalerites were selected for these comparisons : - chalcopyrites previously studied by Harris et al. (11) were analyzed again to demonstrate the reproducibility of both techniques used ; owing to Zn-Fe replacement and presence of minor elements in sphalerites, these specimens were studied to show the influence of composition changes both on intensity measurements and concentration calculations.

Experimental

EPMA

The computer controlled CAMECA microprobe (Camebax-Microbeam type) equipped with four wavelength dispersive spectrometers (WDS) and installed at the joint B.R.G.M.-C.N.R.S. (Bureau de Recherches Géologiques et Minières - Centre National de la Recherche Scientifique) laboratory was used. According to the usual notations used with EPMA, the X-ray intensity for element Z, namely I_Z denotes the number of photons (counts) measured per second per nA electron beam intensity, while N_Z denotes the total number of counts measured for the experimental conditions. K_Z designates the X-ray intensity measured at the surface of the specimen (sp) normalized to that of a standard (st), containing the element Z. The weight fraction C_Z is then given by :

$$K_z = C_z \frac{\int_0^\infty \phi^{sp}(\rho z) \exp\left(-\frac{\mu}{\rho} \rho z \operatorname{cosec}\right)^{sp} d\rho z}{\int_0^\infty \phi^{st}(\rho z) \exp\left(-\frac{\mu}{\rho} \rho z \operatorname{cosec}\right)^{st} d\rho z} \qquad [1]$$

where $\phi(\rho z)$ expresses the distribution with depth of the number of generated X-ray photons resulting from inelastic scattering of the incident electrons with the solid ; μ/ρ is the mass attenuation coefficient of the matrix of density, ρ, for the wavelength of analyzed photons and Θ is the take-off angle of the spectrometer. Abundant literature is available about the formalism expressing the interaction of electrons with solids. In practice, the integrals in equation [1] are calculated by means of three analytical expressions, known as the Z.A.F. correction factor including the atomic number function, Z, (backscattering and energy losses of electrons), the absorption, A, and fluorescence, F, functions expressing the interactions between the generated photons and the matrix. To obtain the weight percent concentrations, the measured X-ray intensities were corrected with the model proposed by Henoc et al. (12) and included in the software package for data acquisition and processing available with the EPMA.

For data acquisition, 6 and 15 sec. counting times were used for major and minor element analyses respectively ; 20 or 30 sec. were used for trace element analyses. The background intensity was derived from two successive measurements on each side of the analyzed peak. Reference compounds and X-ray emissions were : pure Cu (Cu Kα), pure Ag (Ag Lα), pure Cd (Cd Lα), pure Ge (Ge Lα), pure Se (Se Kα), pure Fe (Fe Kα), AsGa (As Lα, Ga Kα, Ga Lα), HgS (Hg Lα, Hg M), natural $InCuS_3$ (In Lα), ZnS (Zn Kα, S Kα) for sphalerite and FeS_2 (S Kα) for chalcopyrite specimen analyses.

Micro-PIXE

The equipment used was the micro-PIXE facility installed at the Max Planck Institüt fur Kernphysik in Heidelberg (FRG) (3). A 4 MeV energy proton beam was used. The proton beam current was monitored by means of a "Rutherford monitor" allowing the specimen to be irradiated with a fixed number of protons, regardless of drift in incident beam current. A ~150 pA proton beam intensity and a total of 250,000 Rutherford units were used. Thus, the data acquisition time was approximately 20 min. To prevent backscattered protons from entering the detector and to minimize pile-up of the matrix K X-ray signals, aluminum absorbers were placed between the target and the Si(Li) detector ; 350 µm and 750 µm thick aluminum foils were used for chalcopyrite and sphalerite analysis,respectively.

As with EDS analysis in EPMA, the general approach common in PIXE is to construct a digital model of a spectrum (peaks and continuum background) and then to vary its parameters to achieve a best fit to the measured spectrum. Intercomparisons of spectral data processing techniques in PIXE analyses have been reported (8). In the present work, data handling and reduction were carried out at Guelph University - Department of Physics - using a model including background removal, peak intensity measurements from the experimental spectra and expression of the net intensities in terms of weight concentrations. The formalism used has been already discussed (9) (16) (7) (6) and the various models used will be only briefly summarized.

The usual approach for peak intensity above the continuum emission used in EDS analysis with EPMA consists in subtracting from the experimental data a theoretical representation of the continuum energy spectrum (17). In micro-PIXE, which is at a much earlier stage of development, most workers have so far used empirical models to describe the continuum background which has to be subtracted from the measured spectrum. The disadvantage of this approach is that the parameters used in the analytical function are not universal, but, are specific to the instrumental and experimental conditions used. An alternate approach to the background intensity removal used in EDS analysis with the EPMA consists of digital filtering using a "top-hat" filter (9) (15). The major advantage of this method is that no theoretical or empirical expression is required to describe the

form of the continuum. The only assumption made is that the continuum varies linearly within any narrow region of the analyzed energy domain. Use of digital filtering in the context of PIXE spectra was first reported by Maxwell et al. (16). In their approach, which is used here, a theoretical model spectrum is fitted to the experimental spectrum by the non-linear least squares method ; the model consists of Gaussian peaks whose positions and widths are related to their energies through calibration expressions which contain four parameters descriptive of the spectrometer. During the fit, these four parameters, together with the heights of the main Gaussian for each element, are varied to minimize the chi-squared. In each iteration it is the digitally filtered spectra that are compared, hence no recourse is necessary to a model for the continuum. A data-base of the X-ray energies and relative intensities is used by the code in constructing the model spectrum.

When the entire experimental spectrum (4-26 keV) was fitted, the quality of fit was markedly less than optimum, and perhaps indicative of a slight non-linearity in the energy calibration ; this caused some under-estimate of peak areas for the heavier elements (Ag, Cd, In), but the effect was not a systematic one. Hence, in most cases a second fit was done to a shorter region of interest (18-26 keV). The Ag, Cd and In data were from this fit.

For data processing in EDS analysis with the EPMA, least-squares fitting methods are generally applied by using experimental spectra of pure elements rather than mathematical descriptions of the X-ray lineshapes. This approach is also feasible in micro-PIXE, but has seen less used than the alternative of modelling the peaks. For both approaches using either theoretical or experimental reference data, a knowledge of all elements present in the analyzed compound is required to take into account the overlap between X-ray lines in order to obtain accurate peak intensity measurements from the least-squares fitting procedure.

For a thick homogeneous target the yield Y (Z) of X-rays from an element Z of weight concentration C_Z and atomic mass A_Z is given by (6) :

$$Y(Z) = N\, C_Z \frac{N_{av}\, \omega_Z\, b_Z\, \varepsilon_Z}{A_Z} \int_{E_o}^{O} \frac{\sigma_Z(E)\, T_Z(E)\, d\,E}{S(E)} \qquad [2]$$

where ω_Z denotes K (or L) X-ray fluorescence yield, b_Z the fraction of K (or L) X-rays in the Kα (or Lα) line, ε_Z the absolute detection efficiency and N the number of incident protons with energy, E_o, N_{av} is Arogadro's number. In the integration over energy, $\sigma_Z(E)$ denotes the ionization cross section, $T_Z(E)$ is the attenuation (absorption) of the number of photons generated by the matrix, and S(E) in the matrix stopping power (energy loss).

Equation [2] may be expressed as

$$Y(Z) = N\, C_Z\, \varepsilon_Z\, I(Z, M) \qquad [3]$$

where

$$I(Z, M) = \frac{N_{av}\, \omega_Z\, b_Z}{A_Z} \int_{E_o}^{o} \frac{\sigma_Z(E)\, T_Z(E)\, d\,E}{S(E)} \qquad [4]$$

I (Z, M) is the integral of X-ray production along the proton path.

Equations [2] and [4] are similar to those used to express the X-ray intensity resulting from the electron bombardment including the ionization cross-section for the analyzed element and the attenuation and stopping power by the matrix M.

The concentration C_Z of the analyzed element may be derived from the measured yield Y(Z) through an absolute calculation of the integral in equation [2] using a data base with a measured or calculated absolute efficiency for the detector. In practice, a comparative method is preferred.

Let I (Z, sp) and I (Z, st) denote the integrals in equation [2] for both the specimen and the standard. Thus, the concentration is given by :

$$C_Z = \frac{Y^{(Z,\,sp)}_{meas}}{Y^{(Z,\,st)}_{meas}} \cdot \frac{I(Z, st)}{I(Z, sp)} \qquad [5]$$

where $Y^{(Z,\,sp)}_{meas}$ and $Y^{(Z,\,st)}_{meas}$ are the measured intensities characteristic of the analyzed element within the unknown and the standard. The integrals I (Z, sp) and I (Z, st) are computed using fundamental parameters to calculate the ionization cross section, the attenuation coefficient and the stopping power. This approach has the advantage of partial cancellation of data base errors.

The expression [5] for micro-PIXE is equivalent to equation [1] for EPMA. The matrix integrals I(Z, sp) and I(Z, st) express the mechanisms of photon production and emission within the unknown specimen and the standard as does the $\phi(\rho z)$ distribution function or the analytical Z.A.F. expressions.

Micro-PIXE calculation based on the use of standards has been reported (2). When a very large number of matrices are concerned, it may be difficult to obtain a sufficient number of reference compounds containing the elements of interest at trace concentration levels, homogeneously distributed within the matrices. Moreover, the use of pure elements as standards will induce large differences in counting rates and statistics for the measured intensities which can be inconvenient experimentally and carries the potential for error.

A different approach, which is something of a compromise between the absolute method and that of elemental standards has been developed for mineralogical applications (7). It is somewhat similar to the method known in EPMA analysis as "standardless quantitative analysis" or "minimum standard analysis" (1).

Equation [3] may be rearranged by splitting off the terms dependent on the matrix from those depending only on the instrumental and experimental factors. The absolute detection ε_Z may be written as

$$\varepsilon_Z = \frac{\Omega}{4\pi} \exp(-\mu x)_{Al}\, \varepsilon^{i}_{Z} \qquad [6]$$

where Ω is the solid angle of the detector, the exponential term expresses the attenuation by the aluminum filter with thickness X and ε^{i}_{Z} is the intrinsic efficiency of the detector.

Both the solid angle and the proportionality constant between the Rutherford backscatter count can be absorbed into an experimental parameter H such that

$$Y(Z, M) = H\, C_Z\, I(Z, M)\, \varepsilon^i_Z \exp(-\mu x)_{Al} \qquad [7]$$

H was obtained by analysing a synthetic $(Fe, Pd)_9\ (S, Se)_{11}$ compound prepared at CANMET (Canada Centre for Mineral and Energy Technology). In this exercise Y(Z, M) was measured, I(Z, M) computed from the data base (14,15), ε^i_Z calculated from the detector specifications and $\exp(-\mu x)_{Al}$ calculated from the nominal aluminum thickness and from attenuation coefficients (14). The result was H = 0.0277.

Silver bearing chalcopyrite

The two analyzed specimens were massive chalcopyrite ($CuFeS_2$) from the Hilton Mine (Northwestern Queensland, Australia) and Izok Lake deposit (Northwest Territories, Canada). Silver concentrations, obtained by means of EPMA and micro-PIXE, were already reported (11) and showed Ag concentrations ranging from 1500 to 2900 ppm (Hilton Mine) and from 260 to 560 ppm (Izok Lake). Other samples from the same deposits were selected for the present study in order to verify the reproducibility of micro-PIXE data and the reliability of EPMA data obtained by varying instrumental and experimental factors.

With EPMA, silver was analyzed by measuring the Ag Lα X-ray intensity induced by electron beam energies of 15, 20 and 30 keV successively. The continuum intensity was derived from two measurements carried out on each side of the Ag Lα peak. Pure silver was used as standard. For each specimen, ten measurements were repeated for the three experimental conditions used.

As shown in table 1, the calculated Ag concentrations from EPMA analyses remained independent of the primary beam energy for both analyzed specimens, indicating a homogeneous distribution of Ag versus depth. Both the statistical precision of intensity measurements and the standard deviation of the data remained in the same order of magnitude indicating a Ag solid solution in both chalcopyrites. The average silver concentrations are 1430 ± 200 ppm for the Hilton Mine sample and 410 ± 150 ppm for Izok Lake sample respectively.

The same specimens were analyzed by means of micro-PIXE induced by a 4 MeV proton beam of 150 pA intensity. Data acquisition time was about 20 min and Ag Kα emission was used for quantitative analysis. The theoretical composition of $CuFeS_2$ was used for data manipulation including determination of peak intensities during the fitting procedure and calculation of the Ag Kα yield for the matrix. A single measurement was carried out for each specimen.

As shown in table 1, EPMA and micro-PIXE data are in good agreement. For the Hilton Mine specimen, the unweighted mean EPMA result of 1433 ppm is within 2 % of the PIXE result. These results are also consistent with results already reported concerning EPMA and micro-PIXE analysis of different samples of chalcopyrite originating from the same deposits (5). For the Izok Lake specimen (EPMA Ag content 410 ppm) the Ag percent difference reaches 18 % but this is acceptable taking into account the lower silver content which is close to the minimum detection limit (MDL) for the experimental conditions used with EPMA. A 3σ criterion was used to calculate the minimum detection limit C_{MDL} for EPMA according to the usual relation :

$$C_{MDL} = \alpha\, 3\, \sqrt{N_B}/N_T \qquad [8]$$

where N_B is the total number of counts for the continuum at the analyzed energy (wavelength), N_T is the total number of counts for the standard and α is the coefficient taking account of the "matrix effect" resulting from the interactions of the incident electrons and generated X-ray photons with the matrix. For the micro-PIXE the C_{MDL} limit of detection was derived from equation [7] where the measured intensity Y(Z, M) was set to 3 times the background intensity. As shown in table 1, the MDL for Ag in $CuFeS_2$ with the micro-PIXE (~ 30 ppm) is better by a factor of ~10 as compared to the EPMA detection limit (from 300 to 400 ppm) for the experimental conditions used.

Table 1 - EPMA and micro-PIXE analyses of Ag and In in chalcopyrites

	Hilton Mine	Izok Lake	
EPMA			
Ep	C(Ag) (ppm) (Ag Lα)	C(Ag) (ppm) (Ag Lα)	C_{MDL} (ppm)
15 keV*	1250 ± 220	430 ± 150	400
20 keV*	1610 ± 190	410 ± 190	310
30 keV**	1440 ± 200	390 ± 105	300
Average	1433 ± 200	410 ± 150	
micro-PIXE			
	(Ag Kα)	(Ag Kα)	
4 MeV	1470 ± 40	335 ± 20	32

	Hilton Mine	Izok Lake	
EPMA			
	C(In) (ppm)	C(In) (ppm)	C_{MDL} (ppm)
20 keV**	n.d.	n.d.	440
micro-PIXE			
4 MeV	36 ± 15	74 ± 22	26

*Counting time = 30 s.
**Counting time = 20 s.
n.d. = not detected.

As also shown in table 1, a factor of 20 is obtained for the In limit of detection in chalcopyrite. Indium concentrations of 36 ± 15 and 74 ± 22 ppm have been detected by micro-PIXE in the Hilton Mine and Izok Lake chalcopyrites respectively. It is interesting to notice the reproducibility of the micro-PIXE data even at concentration levels approaching the statistical limit of detection by comparing the present results to those previously obtained by Harris et al. (11) who obtained In concentrations of 38 and 72 ppm respectively.

Sphalerite

EPMA

Sphalerites (Zn,Fe...)S from ten different massive-sulfide ore deposits were selected. Point qualitative analyses were carried out using a step-by-step automated data acquisition procedure as previously described (10). LiF, PET and TAP monochromators were used and spectra are given in figure 1. The analyzed specimen, was from the Saint Salvy deposit (Tarn, France). Due to the the high sensitivity of the spectrometers, multiple reflections up to the seventh order could be qualitatively recorded in the case of the major Zn constituent of the matrix. Multiple orders of reflection can also be recorded in the case of minor elements as shown in figure 1 for Fe and Cu. Obviously the detectability of low intensity peaks resulting from multiple orders of reflection will be increased in the quantitative analytical procedure as compared to the qualitative data acquisition approach.

Due to the large number of impurities which can be present in sulfides with various levels of concentrations, there is no general rule for experimental conditions to be used for trace element analyses. The beam energy must be optimized for maximum sensitivity, depending on the X-ray energy analyzed and the matrix composition.

Theoretical K, L and M spectra for trace elements which will be considered in the present study are indicated in figure 1. Usually, elements with an atomic number lower than 30 are analyzed via their K spectrum, elements with atomic number ranging from 31 (Ga) to 72 (Hf) are characterized by their L spectrum and elements with higher atomic number by their M spectrum. However it may be necessary in some instances to analyze some of the elements by their high energy X-ray emission to avoid overlaps between peaks or when the efficiency of the monochromator is too low to obtain a sufficient statistical precision for intensity measurements.

As an example, the Hg Mα peak is analyzed by means of the PET monochromator (Fig. 1). As this spectrometer is of the linear fully focussing type, the PET crystal is placed at a long distance from the X-ray source for the Bragg position corresponding to Hg Mα (2.19 keV, i.e. 5.65 Å) and the measured counting rate is very low. Further, for the low energy Hg Mα emission, the matrix effect is very large. For Hg Mα, the minimum limit of detection, (taking account of the interaction of the X-ray photons with the matrix) leads to a corrected minimum detection limit, C_{MDL}, is ~ 1500 ppm. Thus, due to the low counting rate and the large correction factor, small statistical fluctuations affecting the peak intensity

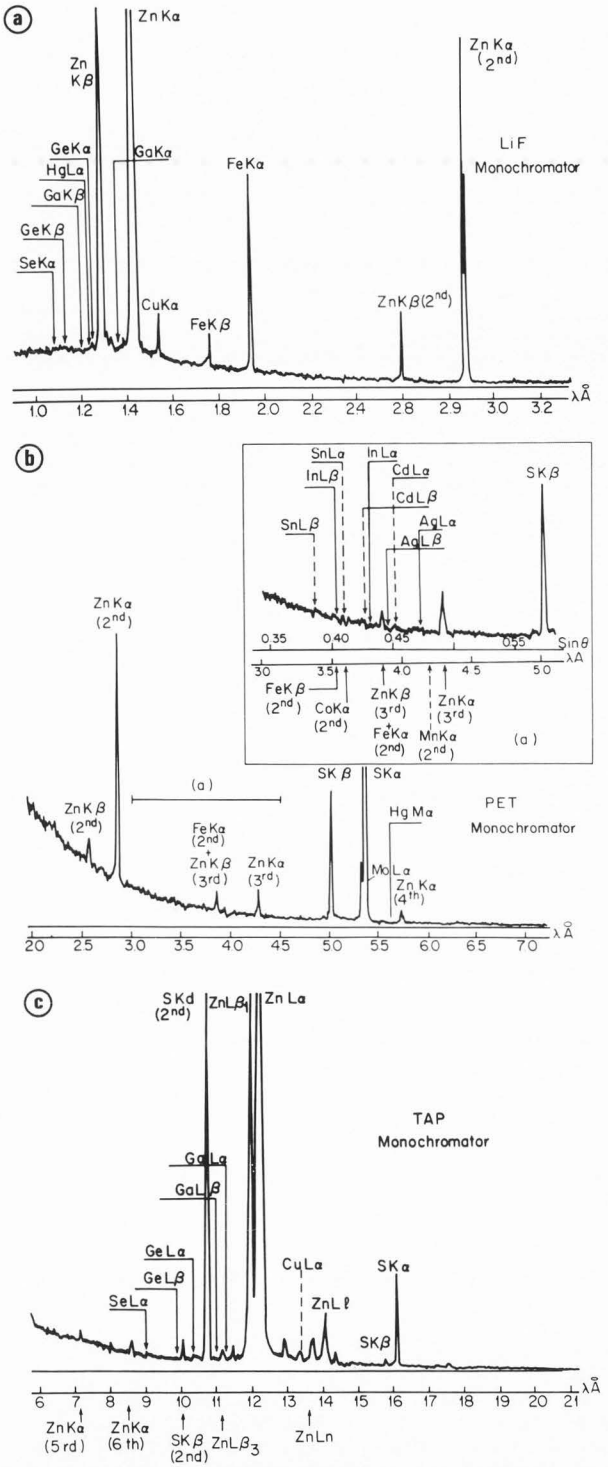

Figure 1 - Automated qualitative analysis (WDS) of a ZnS specimen with EPMA using (a) LiF, (b) PET and (c) TAP monochromators. The three monochromators are moved simultaneously step by step ; total acquisition time is about 10 min. X-ray emissions used for trace element analyses are shown.

measurements will induce large uncertainty for the calculated concentration.

Although with different values, similar conclusions can be reached in the case of Ga Lα. Low detection efficiency could be overcome by increasing the counting time but this must be selected in order to satisfy one of both objectives ; to get a sufficient number of point analyses for statistical data processing leading to an average concentration of the analyzed elements within the matrix (the minimum detectable limit is thus defined) to get a given limit of detection ; but increasing the counting-time in order to reach a particular statistical precision can lead to possible beam damage. The maximum dose of irradiation must be evaluated for each analyzed matrix.

Thus, rather than to extend the counting time, it may be preferable to use a higher energy emission. Such an approach is required when Ga and Hg are present simultaneously. As shown in figure 2 the Hg Mα (2nd order) overlaps the Ga Lα peak and justifies the choice of the energetic Ga Kα peak.

It has been shown (20) that the particular beam energy, E_p, leading to the maximum of the peak to continuum intensity ratio is related to the matrix absorption coefficient $(\mu/\rho)_\lambda$ for analyzed photons of wavelength λ, according to the following relation :

$$\chi = (\mu/\rho)_\lambda \operatorname{cosec} \Theta = \frac{2660}{E_p}^{1.68} \qquad [9]$$

where Θ is the take-off angle of the spectrometer.

The above relation was used to study the mass attenuation coefficient which exhibits large discrepancies among published data (22). The above relation may be used to predict the optimized primary beam energy for each analyzed element. Again, a compromise must be accepted to keep the peak to continuum intensity ratio at an acceptable level for all the analyzed elements within the matrix. In practice, a 20 keV primary beam energy was used. Occasionally a 30 keV primary beam energy was used for comparisons of data from emissions of different energy.

For the analysis of Hg in the ZnS matrix, using Lα, the corrected limit of detection is reduced to 800 ppm as compared to the previous 1400 ppm limit.

Concerning the continuum associated with a given characteristic peak, the location where to measure its intensity must be selected in order to take account of the presence of adjacent peaks. Indeed, it is not possible to use a blank specimen as it would be necessary to have one not only with the same major elements (Zn,Fe...) but also with the same minor and trace elements with the exception of the element to be analyzed. We used the classical approach of deriving the continuum intensity $N_B(\lambda_o)$ at wavelength, λ_o, by linear interpolation from two measurements carried out at wavelength $\lambda_o \pm \Delta\lambda_o$. The value of the $\Delta\lambda_o$ interval must be chosen to prevent distortion of the shape of the continuum distribution due to the presence of peaks. As an example, when measuring the Ga Lα emission with a TAP monochromator (Fig. 2) the shape of the continuum is modified by the presence of Cd Lα (3rd reflection order) and Zn $L\beta_3$ (fundamental) emission. In order to support the approach of measuring the continuum intensity by varying the monochromator position we studied synthetic and natural sphalerite specimens which did not contain the trace element whose X-ray continuum intensity measurement was under investigation.

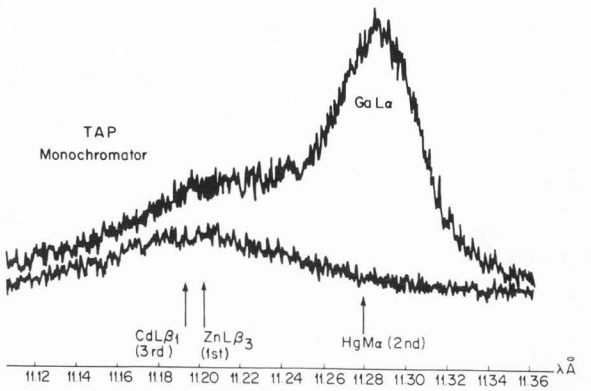

Figure 2 - L spectrum (WDS-TAP monochromator) for Ga in a ZnS matrix.

The X-ray intensity $N_B(\lambda_o)$ was measured at the characteristic wavelength, λ_o, of the element of interest and at wavelengths $\lambda_o \pm \Delta\lambda_o$ successively. For each condition, ten measurements were repeated and averaged. The two sets of measured intensities $N_B(\lambda_o)$ and $1/2\ [N(\lambda_o + \Delta\lambda_o) + N(\lambda_o - \Delta\lambda_o)]$ differed by less than 5 % i.e. less than one standard deviation of the measurements. These experiments were performed in order to determine the $\Delta\lambda_o$ interval making valid the linear interpolation for the continuum intensity measurement for the trace elements in the analyzed sphalerites.

Micro-PIXE

The necessary use of rather thick absorbers (aluminum in the present work) in micro-PIXE has major effects on the low-energy portion of EDS spectra. This is illustrated in figure 3 for the case of a sphalerite specimen from the Chessy deposit (Rhône, France). For a 750 μm thick absorber the Kα/Kβ intensity ratio of Zn is decreased by a factor of about 8 relative to its value in the absence of absorbers. For à 350 μm thick absorber the decrease is rather less, while additional features become apparent. Peaks at 6.9 and 7.8 keV are the ZnKα and ZnKβ escape peaks; the latter effectively masks small amounts of copper although Cu is known to be present from the EPMA work. The former masks Co Kα, which was not detected with EPMA. In one case a small FeKα peak was observed in the micro-PIXE spectra : this was consistent with EPMA. The increased counting rate also leads to pile-up effects as shown in the ZnS spectrum recorded when a 350 μm absorber was used. Three broad weak peaks are observed in the energy range from ~ 17 keV to ~ 20 keV. These peaks correspond to the sum peaks resulting from pile-up effects from the Zn Kα + Zn Kα peaks (8.64 + 8.64 = 17.28 keV), the Zn Kα + Zn Kβ peaks (8.64 + 9.57 = 18.21 keV) and from the Zn Kβ + Zn Kβ peaks (9.57 + 9.57 = 19.14 keV). The presence of the sum peaks resulting from the Zn Kα and Zn Kβ will worsen the detection limit for Mo whose Kα and Kβ transitions occur at 17.48 and 19.61 keV respectively ; even if Mo is not a trace

element in sphalerite, it was recorded in some specimens as molybdenite (MoS_2) inclusions and could be present in other sulfides.

A 750 μm thick Al absorber was used for the sphalerite analyses. Thus, the Fe and Cu concentrations (varying in large proportion from one specimen to another as shown from EPMA data) were not detected with the micro-PIXE. We have evaluated the influence of the minor Fe and Cu concentrations on the accuracy of X-ray yield measurements and calculations for the trace elements within the (Zn,Fe)S and (Zn,Cu)S matrices. Three levels of X-ray energies were considered (Fig. 3a) : the high energy domain containing the Ag Kα, Cd Kα, In Kα emissions, a medium energy domain in which Se Kα and Hg Lα lie and finally the region of Zn Kα, Kβ which includes Ga Kα and Ge Kα

The integrals I(Z, M) were calculated for the elements Cd, In, Ag, Hg, Se, Ge, Ga assumed to be present in a (Zn, Fe)S matrix. For these calculations the Fe concentration was increased from 0 to ~10 % consistent with EPMA data of the sphalerite specimens from various deposits. As shown in figure 4 the integrals I(Z, M) for Ga Kα and for Cd Kα, Ag Kα, Ge Kα and In Kα vary linearly with the Fe concentration in the (Zn,Fe)S matrix but the slope of the linear variation is a function of the energy of the analyzed X-ray photons. These variations result from the attenuation of the photons by the (Zn,Fe)S matrix as illustrated by the diagram in figure 5. The Ga Kα emission is located in front of the K absorption edge of Zn, so that the average absorption coefficient of the matrix will increase when Zn is replaced by Fe and/or Cu leading to a decrease of the Ga Kα integral simultaneously. The average absorption coefficient $\bar{\mu}$, is defined as $\bar{\mu} = \Sigma C_Z \mu_Z$ where C_Z is the weight concentration of the element, Z, with a mass absorption coefficient, μ_Z, for the analyzed X-ray emission.

As the Ge Kα (and Kα lines for elements of higher atomic number) is above the Zn K absorption edge, then the Zn absorption coefficient will be the predominant contribution to the matrix absorption coefficient. A decrease in Fe (or Cu) content, i.e. an increase of the Zn concentration, will lead to a decrease of the Ge integral.

Thus, for analyzed energies lower than the K absorption edge of Zn, the slope of the linear variation of the matrix integral I(Z, M) versus Fe (and/or Cu) concentration in (Zn,Fe)S will be negative and the slope of the linear variation will become positive for energies greater than the absorption edge. However the slope will decrease and tend towards a constant value when the atomic number of the analyzed element increases above Z = 32.

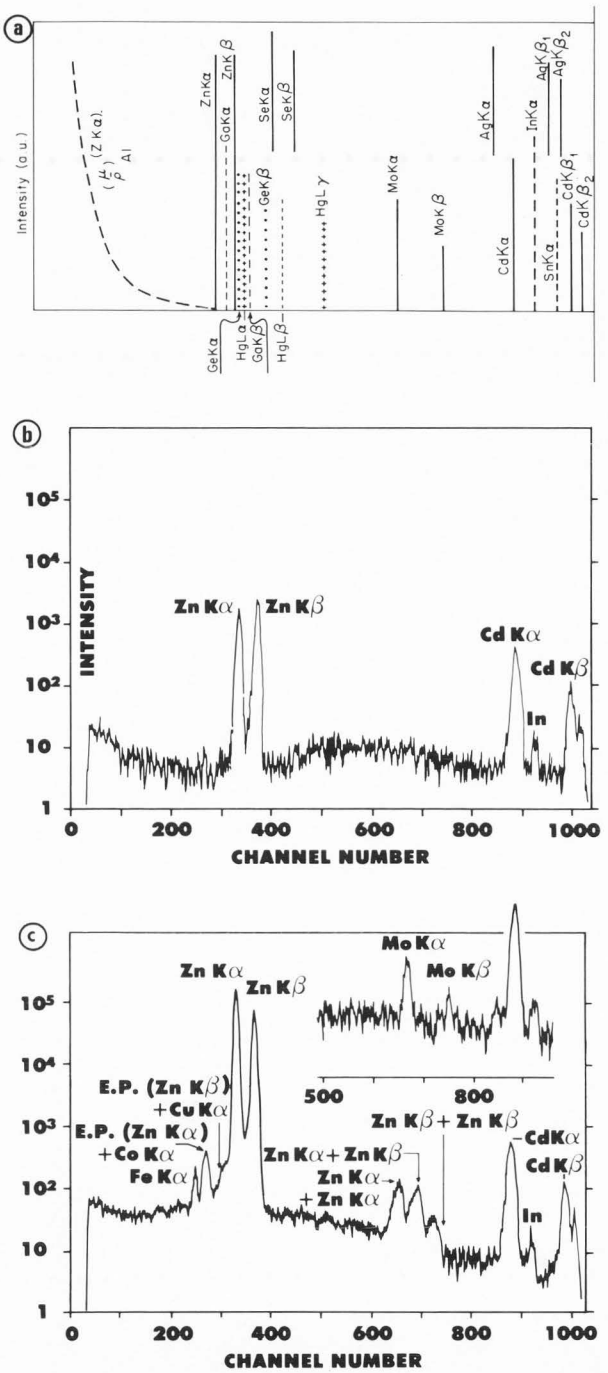

Figure 3 - Qualitative analysis (EDS) of a ZnS specimen with the micro-PIXE :

a) Characteristic X-ray peak energies for the trace elements analyzed in the sphalerite specimens. Also shown is the variation of the absorption coefficient by the Al absorber for X-ray emission with energies lower than Zn Kα.

b) EDS analysis using a 750 μm thick Al absorber in front of the detector. Note the relative intensities of the ZnKα and Zn Kβ peaks.

c) EDS analysis of the same specimen as above using a 350 μm thick Al absorber. Compare the relative Zn Kα and Zn Kβ intensities to those obtained in the previous case. Also note the detection of the Fe Kα, Co Kα and/or escape peak resulting from the Zn Kα high intensity peak, Cu Kα and/or Zn Kβ escape peak and the sum peaks from Zn Kα and Zn Kβ occurring within the energy range of Mo Kα, Kβ peaks.

As shown in figure 5, Cu is also a filter for the Ga Kα and Ge Kα emissions. Some of the analyzed sphalerite specimens containing Ga also contained Cu as shown by EPMA analysis. The Cu concentrations range from ~ 0.2 % (specimen from the Djebel Gustar deposit, Algeria) to ~ 2 % (specimen from Kipuski, Zaire). EPMA analyses showed that small amounts of Cd were also present. The variation of the integrals for Ga Kα when increasing the Fe, Cu and Cd concentrations are shown in figure 6. For a given amount of Fe, the Ga Kα integral decreases when the Cu concentration increases and, in a first approximation, the Ga Kα integral remains independent of the Cd concentration.

According to equation [4] the Kα yield for trace elements within the (Zn,Fe)S matrix will also vary linearly with the concentration of the element which can substitute for Zn. Iron being the main minor element encountered in sphalerites, with concentration varying over a large domain, the X-ray yields for the trace elements commonly present in the (Zn,Fe)S matrix were calculated for Fe = 0 and Fe = 10 % weight fraction successively.

Thus, the X-ray yield Y[Z(Zn,Fe)S] for a trace element, Z, incorporated in the (Zn,Fe)S matrix may be expressed as :

$$Y[Z(Zn,Fe)S] = aC_{Fe} + Y(Z,ZnS) \qquad [10]$$

Data in table 2 show the slope, a, and the ordinate at the origin, Y(Z,ZnS) of the linear variations of yield Y[Z(Zn,Fe)S] versus the iron content for some trace elements within sphalerite matrix. Also shown in table 2 are the percent differences between the X-ray yields calculated when 0 % and 10 % of iron are present in the matrix. Thus, assuming that the matrix has the theoretical composition ZnS is a sufficient approximation for Cd Kα, Ag Kα, In Kα... quantitative analysis within sphalerite specimens.

The dependence of the X-ray yield Y(Z, M) upon the matrix composition is obviously controlled by the element exhibiting the highest absorption attenuation coefficient (or fluorescence enhancement). Although the presence of a trace or minor constituent may affect the X-ray yield characteristic of another trace element, it is less important than the effect of a variation of the Zn concentration upon the average mass absorption coefficient for the analyzed energy of element with characteristic X-ray emission located immediately above the K absorption edge of Zn. For analyzed energies lower than the Zn K absorption edge the matrix effect will mainly depend on elements with atomic number < 30 being present in appreciable amounts (mainly Fe and Cu).

Knowledge of the matrix composition is also required to extract the X-ray intensities characteristic of the analyzed trace elements by fitting the experimental spectrum to theoretical spectra for each of the elements present in the specimen. As for matrix integral and X-ray yield calculations, the use of the theoretical ZnS composition may be a sufficient approximation to derive X-ray intensities for some of the trace elements. This approximation may run into problems when overlaps occur between peaks as illustrated in figure 7 where Ga Kα and Zn Kα peaks partly overlap the Zn Kα and Zn Kβ peaks. It is obvious from this illustration that the Ga Kα and Hg Lα peak intensity measurement by the least-squares fitting procedure will only be possible if the model description of the Zn Kα and Zn Kβ peak is extremely accurate. This is not the case since the present model ignores both low energy peak tailing and radiative Auger satellites. An alternative deexcitation mode for a K vacancy is the simultaneous emission of a bound electron and an X-ray photon. This results in the Kβ line having a (KMM) satellite, corresponding to a K-M photon transition with ejection of an M electron. Similarly the Kα line has KLL and KLM satellites. The Zn KMM satellite, in particular, overlaps with the Ga Kα peak. Again, all minor elements which can substitute for Zn, leading to a deviation of the Zn Kα, Kβ spectrum from the pure ZnS spectrum must be known and added to the fitting procedure. As an example, the effect of the matrix composition changes on the measured X-ray intensity has been evaluated in the case of Ga Kα in a (Zn,Cu)S matrix. The specimen (from Kipushi, Zaire), contains Ga, Cd, and Cu ; although its concentration is ~ 2 wt %, Cu was not detected with the microPIXE due to absorption by the Al filter.

The Ga Kα and Cd Kα intensities from the micro-PIXE spectrum were calculated using both theoretical and measured compositions derived from EPMA data in the least-squares procedure. The X-ray yields for Ga Kα and Cd Kα were also calculated for both compositions of the matrix. For these calculations we used the integral values derived from the curves in figure 6. The Ga and Cd concentrations were then derived from measured intensities and calculated

Table 2 - Some results of X-ray yield calculations for trace elements in (Zn,Fe)S matrix.
The yield of element Z is

$$Y[Z(Zn,Fe)S] = a\,C_{Fe} + Y(Z,ZnS)$$

and

$$\frac{\Delta Y}{Y} = \frac{Y[Z(Zn,Fe)S] - Y(Zn,ZnS)}{Y(Z,ZnS)}$$

Element Z	X-ray emission	Photon energy keV	Y(Z,ZnS)	a	$\frac{\Delta Y}{Y}$ %
Ga	Kα	9.25	0.167	-0.310	20.3
Ge	Kα	9.88	0.140	0.063	-5.0
Se	Kα	11.22	0.606	0.253	-4.5
Mo	Kα	17.48	3.307	0.633	-2.1
Ag	Kα	22.16	2.055	0.265	-1.4
Cd	Kα	23.17	1.709	0.274	-1.7
In	Kα	24.21	1.411	0.139	-1.0
Sn	Kα	25.27	1.171	0.138	-1.3
Hg	Lα	9.99	0.0549	0.02	-5.1

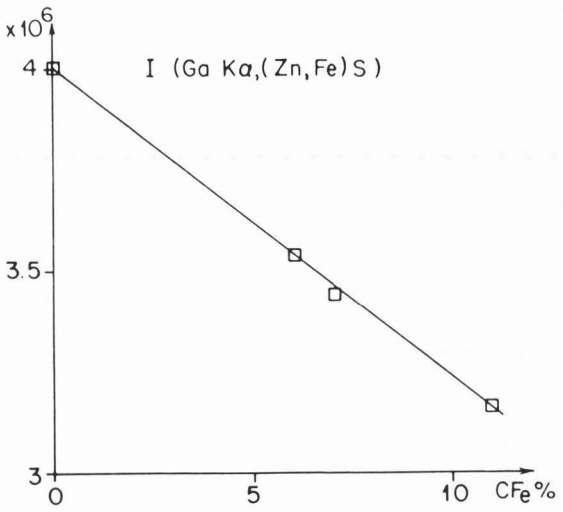

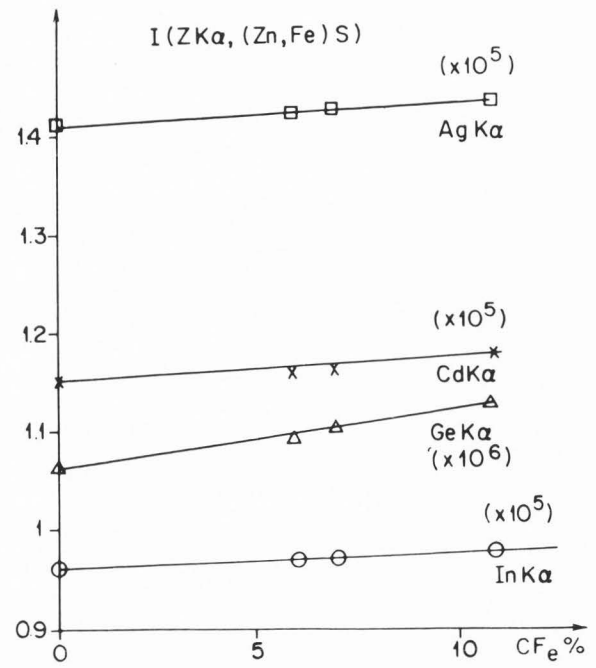

Figure 4 - Matrix integrals I(Z, M) for trace elements, Z(Ga, Ge, Ag, Cd, In) calculated by varying the Fe weight fraction within the (Zn, Fe)S matrix.

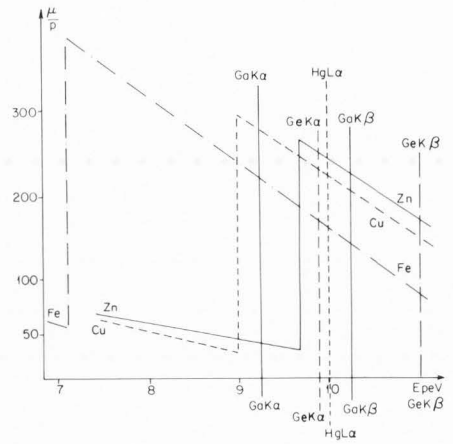

Figure 5 - Mass absorption coefficients of the major (Zn) and minor (Fe, Cu) constituents of the matrix for the Ga and Ge K emission spectra and Hg Lα emission.

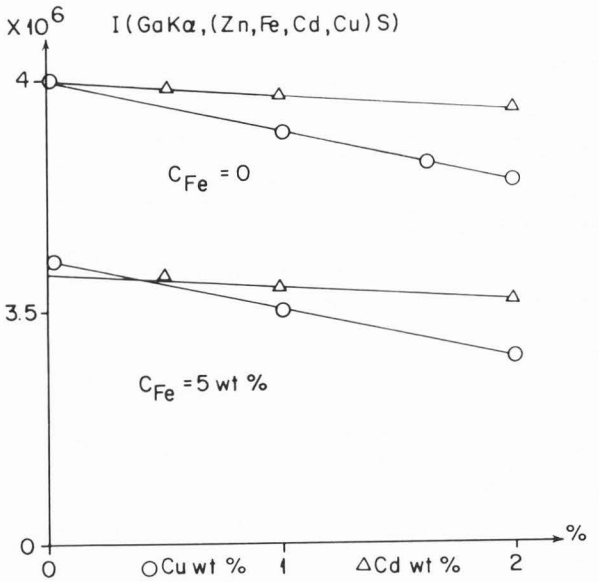

Figure 6 - Calculated matrix integral for Ga as a function of the Cu and Cd concentrations within a ZnS and (Zn,Fe)S matrices.

Figure 7 - Part of the micro-PIXE (EDS) experimental spectrum of a ZnS specimen containing Ga and Hg as impurities (Djebel Gustar, Algeria) ; Cu (~ 0.2 %) is not detected due to the 750 μm thick Al absorber.
RA (KMM) : Radiative Auger satellite (see text).

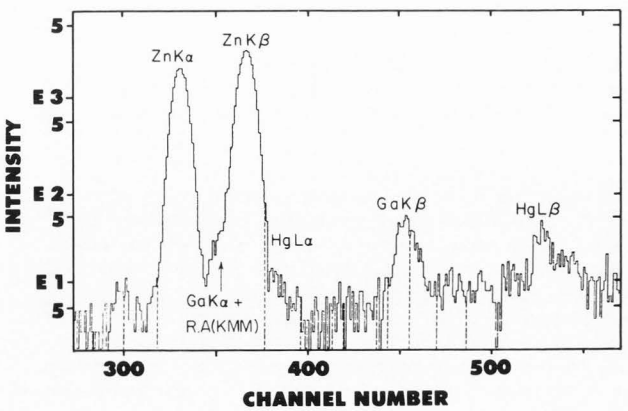

yields. As shown in table 3 the Cd intensity, yield and concentrations remain constant when matrix composition changes due to minor elements substituting for Zn are neglected. The Ga results are very sensitive to matrix composition changes, however, as shown in table 3 ; the relative difference in the calculated Ga Kα intensities is much higher than the relative difference in the calculated yield due to the matrix composition used for the data reduction procedures. Moreover, the relative difference for the calculated concentrations is in the same order of magnitude as the relative difference observed for intensity measurements. Thus, these results indicate that the least-squares fitting technique is more sensitive to the uncertainty in the matrix composition than the X-ray yield calculation. Error in the former arises from matrix uncertainties, from the approximations used to model peaks and from the background removal procedure.

Similar conclusions were drawn when processing data for Ge and Hg impurities in sphalerites. Results for Ge exhibit higher discrepancies with matrix composition than results for Hg.

As reported earlier and illustrated in figure 3, the use of an aluminum absorber in front of the detector limits the atomic number of the detectable elements. For the available instrumental conditions, elements with atomic number < 30 were not detected. Thus, for elements such as Cd, In, Ag, Se, Mo and Hg the theoretical ZnS composition will be used for data processing while for Ga and Ge some data will be processed using the true composition derived from EPMA analyses.

Table 3 - Variations of calculated intensity, X-ray yield and concentration for Ga and Cd as a function of the (Zn,X)S matrix composition used for calculations

Ga Kα in sphalerite from Kipushi (Zaire)

Matrix composition used in the fitting and yield calculations	Intensity	Yield	Concentration wt %
Theoretical ZnS composition (1)	2631 ± 104	0.167	1.57 ± 0.06
Observed true composition (EPMA data) (2)	2140 ± 88	0.163	1.31 ± 0.07
$\frac{\Delta I}{I}, \frac{\Delta Y}{Y}, \frac{\Delta C}{C}$ %	18 %	2.4 %	16 %

Cd Kα in sphalerite from Kipushi (Zaïre)

Matrix composition used in the fitting and yield calculations	Intensity	Yield	Concentration (ppm)
Theoretical ZnS composition (1)	6046 ± 158	1.709	3538 ± 90
Observed true composition (EPMA data) (2)	6145 ± 156	1.724	3564 ± 90
$\frac{\Delta I}{I}, \frac{\Delta Y}{Y}, \frac{\Delta C}{C}$ %	1.6 %	0.9 %	0.7 %

(1) Theoretical composition : Zn = 0.67 - S = 0.33

(3) Composition derived from EPMA data : Zn = 0.632 - Cu = 0.02 - Ga = 0.02 - Cd = 0.004 - S = 0.324

Results

Cadmium and Indium

Sphalerites from ten deposits were analyzed for Cd and In. The average value of ten measurements with the EPMA are given in table 4 ; for the micro-PIXE, only one or two analyses were performed but always very close to the areas previously analyzed with the EPMA.

For Cd the discrepancy between the two sets of data ranges from ~ 4 % to ~ 15 % but can reach 30 % for some samples (Boumadine, Saint Veran and Djebel Gustar) but it must be considered that the repartition of Cd is very inhomogeneous and that the number of analyses with the micro-PIXE is insufficient to average this erratic distribution.

As for indium, with the EPMA it was not detected with the 3σ criterion but, as Cd is always present, the continuum intensity measurement was influenced by the presence of the close Cd Lβ (1st order), thus diminishing the peak/continuum ratio.

Germanium and silver

A specimen from the Saint-Salvy deposit (Tarn, France) was analyzed with the EPMA before micro-PIXE analysis. Fe, Cu, Cd, Ge and Ag were detected as minor and trace elements within the sphalerite. Seventy point EPMA quantitative analyses were carried out at ~ 20 μm steps distributed along the axis, xx', at the surface of the specimen. The location of some of the analyzed points are made visible by the contamination spots induced by the electron irradiation as shown on the backscattered electron image in figure 8. The graph, in figure 9 shows concentration variations of minor - and trace elements, for the 70 points along xx'. The distribution of these elements is heterogeneous ; Fe and Cd maximize while Ge and Ag minimize simultaneously.

Four regions, marked I, II, III and IV along the xx' axis in figure 9 were selected for microPIXE analyses. Due to the heterogeneous distribution of the elements, five EPMA points analyses (20 μm steps along the yy' axis shown in figure 8) were again carried out as shown in figure 9 in order to verify that for each analyzed area the composition changes were small enough to allow comparisons of EPMA and micro-PIXE quantitative data.

Table 4 - Comparisons between EPMA and microPIXE data : Cd and In in sphalerites from various localities

Origin of the specimens	Cd (ppm)		In (ppm)	
	EPMA	micro-PIXE	EPMA	micro-PIXE
Ivigtut (Greenland)	1800 ± 250	1739 ± 70	n.d.	335 ± 40
Orpierre (Hautes-Alpes, France)	1220 ± 180	1470 ± 70	n.d.	n.d.
La Rabasse (Hérault, France)	7010 ± 280	6372 ± 130	n.d.	250 ± 40
Cupra (Québec, Canada)	4050 ± 340	3580 ± 100	n.d.	153 ± 35
Chessy (Rhône, France)	3290 ± 310	3158 ± 70	n.d.	129 ± 30
Boumadine (Morocco)	9300 ± 390	6480 ± 140	n.d.	780 ± 80
Assif Imiter (Morocco)	7340 ± 300	6319 ± 120	n.d.	75 ± 25
Kipushi (Zaïre)	3750 ± 340	3600 ± 100	n.d.	n.d.
Saint Veran (Hautes-Alpes, France)	1630 ± 320	2450 ± 80	n.d.	n.d.
Djebel Gustar (Algéria)	2990 ± 310	2180 ± 80	n.d.	n.d.

n.d. = not detected.

With EPMA the elements Zn, Fe, Cu and S were characterized by their Kα X-ray emission, and Cd, Ge, and Ag by their Lα emission. With the micro-PIXE, S, Zn, Fe and Cu were not measured (Al absorber) ; Cd, Ge and Ag were analyzed by their K spectrum.

The EPMA data indicated that the Fe concentrations varied from ~1.75 % to ~3.5 % in the vicinity of the areas analyzed with the micro-PIXE. As previously discussed (Figure 4) the matrix integrals for Cd, Ag, and Ge vary slowly with the Fe content.

Figure 9 - Quantitative analyses with the EPMA, by 20 micron step along the xx' axis shown in figure 8.

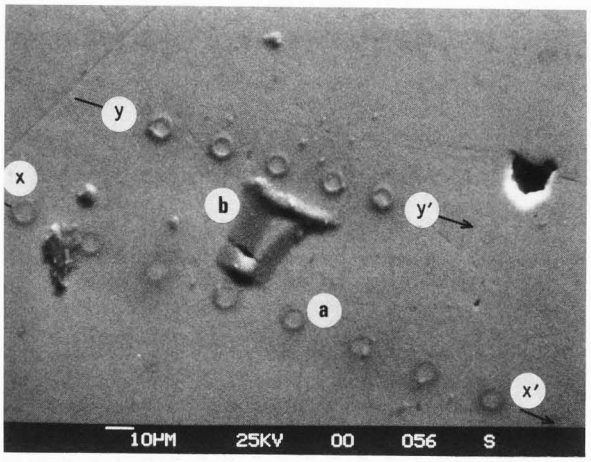

Figure 8 - Electron image of the sphalerite from Saint-Salvy (Tarn, France) showing contamination spots induced by electron and proton beam bombardments after EPMA and micro-PIXE analyses.

a) Analyzed spots with EPMA, by 20 micron step, before micro-PIXE analysis (70 points were analyzed along the xx' axis).
b) Area analyzed with the micro-PIXE : 4 areas were analyzed.
c) Analyzed areas with EPMA after micro-PIXE analysis.

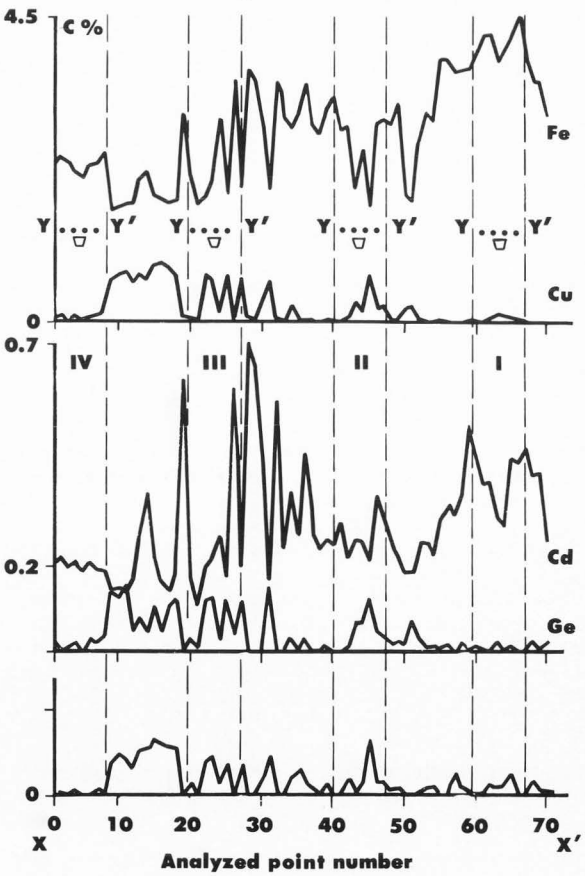

Thus, an average of 2 wt % Fe was used in the X-ray yield calculation for the trace elements of interest. A small amount of Cu (maximum of ~ 0.5 %) was also locally detected with the EPMA but was neglected for micro-PIXE data manipulation.

Comparisons of EPMA and micro-PIXE data are shown in table 5. The EPMA data are the average of five measurements carried out at a small distance from the areas analyzed with the micro-PIXE excepted for Ag and Ge in areas I and IV respectively. In these later Ag and Ge were only detected on some of the five previous points, making impossible the averaging of the data. In table 5 only the highest values for Ag and Ge locally detected in areas I and IV are reported between brackets. The variations in composition between the four areas analyzed with the micro-PIXE are consistent with the variations shown by EPMA data (xx' axis in figure 9). Comparing quantitative data obtained from both techniques, an average percent difference of 12 % is observed for Cd with concentration of ~2000 ppm. The percent difference is ~ 20 % for Ag concentrations of ~ 500 ppm and ~ 15 % for Ge with concentrations of ~ 1000 ppm.

Gallium, mercury and selenium

The sphalerites originating from Kipushi (Zaire), Djebel Gustar (Algeria) and Saint-Veran (Hautes-Alpes, France) were analyzed. The EPMA showed that Cu and Fe were present in the three samples. Cd, Ga, Hg and Se were detected by both the EPMA and the micro-PIXE.

Gallium : Cadmium and Ga are the two impurities detected with the micro-PIXE in the specimen originating from the Kipushi deposit. EPMA and micro-PIXE data for Cd are in good agreement as shown in table 4. The EPMA also showed that Cu is present with a concentration of ~2 wt % but was not detected with the micro-PIXE (effect of the Al absorber). According to the previous study of the matrix integral and yield calculations (see fig. 6) the presence of Cu cannot be neglected in the data processing for Ga Kα derived from micro-PIXE measurements. The presence of Cu was neglected in data processing for Cd. Micro-PIXE analyses were carried out for two different proton beam locations. Then, around each area, five EPMA measurements were carried out and averaged. The percent differences for Ga concentrations derived from both techniques are 18 % and 30 % for the two analyzed areas respectively. However, the relative variations of the Ga concentrations at the two analyzed locations derived from EPMA data (2.30/1.8 = 1.27) and micro-PIXE data (1.65/1.47 = 1.12) are consistent. The same conclusions can be drawn for Cd analysis as reported in table 6.

For the specimen originating from the Djebel Gustar deposit, Cu, Cd, Ga and Hg are present simultaneously and EPMA data indicated that Cu has an average concentration of ~ 0.2 %. This element was neglected in the micro-PIXE data handling for Cd, Ga and Hg. Four areas were randomly selected for micro-PIXE analyses. The observation of the contamination spots which developed during proton beam irradiation allowed the selection of the same areas for EPMA analyses. Five EPMA measurements were carried out

Table 5 - EPMA and micro-PIXE analyses of the sphalerite from the Saint Salvy deposit (Tarn, France)

Area	EPMA Fe* (‰)	EPMA Cu* (ppm)	Cd (ppm) EPMA	Cd (ppm) micro-PIXE	Ag (ppm) EPMA	Ag (ppm) micro-PIXE	Ge (ppm) EPMA	Ge (ppm) micro-PIXE
I	3.5	500	2690 ± 210	2874 ± 267	l.d. (700)**	215 ± 27	l.d. (380)**	n.d.
II	1.75	5950	1850 ± 200	2133 ± 78	537 ± 50	502 ± 37	1330 ± 75	964 ± 171
III	2.5	5314	1980 ± 200	2249 ± 89	630 ± 44	487 ± 38	1020 ± 75	1028 ± 157
IV	2.2	510	1990 ± 200	1630 ± 70	l.d. (400)**	52 ± 17	l.d. (450)**	236 ± 114

*Not detected with the micro-PIXE due to the presence of the Al absorber.

**Denotes the highest value locally detected.

n.d. = not detected.

l.d. = locally detected.

Table 6 - EPMA and micro-PIXE analysis of the sphalerite from the Kipushi deposit (Zaire)

Cu(1) (%) EPMA	Fe(1) (ppm) EPMA	Cd (ppm) EPMA	Cd (ppm) micro-PIXE	Ga (%) EPMA(2)	Ga (%) micro-PIXE(3)
		3330 ± 246	3535 ± 90	2.30 ± 0.04	1.65 ± 0.06
2.01	310	3930 ± 250	3760 ± 95	1.80 ± 0.05	1.47 ± 0.06

(1) Not detected with the micro-PIXE (Al absorber).

(2) Ga Lα emission used for analysis.

(3) Ga Kα emission used for analysis.

by steps of ~20 µm as previously done for the specimen from the Saint-Veran deposit (Fig. 8). The diagrams in figure 10 illustrate the Cd, Ga and Hg concentrations derived from EPMA measurements for the analyzed areas numbered II and III in table 7 respectively. These results show that the measured concentrations vary rapidly when the electron beam irradiated two areas separated by only a few tens of microns. This heterogeneity of the trace element distribution is consistent with cathodoluminescence observations previously reported (22). It has been shown that when an unfocused electron beam (20 keV, 100 nA) irradiated an area of ~300 µm in diameter, cathodoluminescence features were visible at the surface of the Djebel Gustar sphalerite. Large dimensioned areas exhibited a deep red luminescence while, locally, parallel narrow domains (a few tens of microns wide) exhibited blue, green or yellow light emission. The cathodoluminescence property changes are the result of the trace element distribution (20).

Owing to the heterogeneity of the analyzed specimen, micro-PIXE data were compared to the average composition derived from the five EPMA measurements when the results exhibited small variations. When the micro-PIXE impact was close to the limit of two domains corresponding to sudden changes in concentration (mainly Ga and Cd), only the two closest EPMA analyses where taken into consideration and averaged. Comparisons are given in table 7.

For the four analyzed regions, EPMA and micro-PIXE data for Cd shows a mean percent difference of ~ 20 %, consistent with results obtained for Cd analysis in the other specimens (see table 4).

In the region labelled I, in table 7, EPMA measurements show two groups of values for Ga. The 1230 ppm value is consistent with the Ga concentration derived from micro-PIXE analysis. As shown in figure 10a for region II the Ga concentrations measured with the EPMA decrease continuously from ~3500 ppm to ~ 0 as a function of the beam location. A Ga concentration of 1560 ppm is obtained by averaging the EPMA data from the two closest beam locations of the analyzed area with the micro-PIXE. The 1560 ppm average value from EPMA is in a good agreement with the micro-PIXE data (1510 ppm). As shown in the figure 10b for the area III an average Ga concentration of 1500 ppm is obtained from five EPMA measurements and is identical to the Ga concentration measured with the micro-PIXE. Within the area IV, a small amount of Ga is detected with the micro-PIXE but not with the EPMA.

For these comparisons, Ga was analyzed using the Ga Lα emission (1.09 keV i.e. λ = 11.29 Å) with the EPMA while the Ga Kα (9.25 keV i.e. λ = 1.34 Å) was used for analysis with the micro-PIXE. The large difference in the analyzed energies may be responsible for the differences observed between EPMA and micro-PIXE data.

For the low energy Ga Lα emission the matrix effect is large. As an example, for a measured K_{Ga} of ~0.75 % (Ga Lα intensity for the specimen normalized to that of the standard) the corrected concentration, C_{Ga}, obtained after applying the ZAF model increased up to 2.20 %. Thus, an error of 10 % for the measured intensity induced a variation of ~30 % for the final concentration, which is the order of magnitude of the percent difference observed between

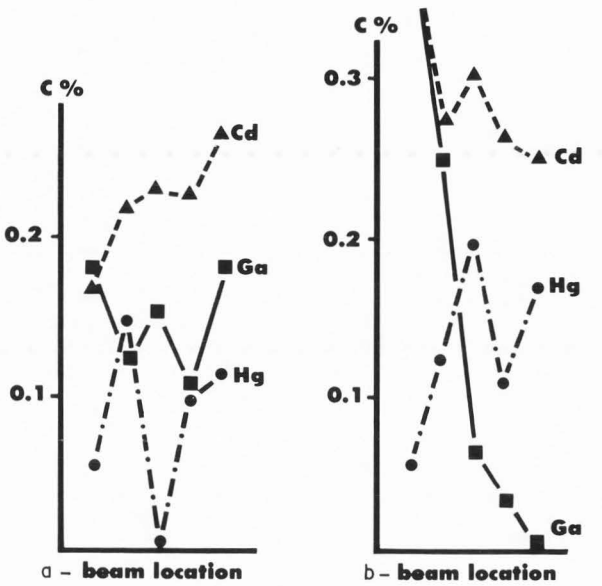

Figure 10 : Cd, Ga and Hg quantitative analysis with the EPMA of the sphalerite from the Djebel Gustar deposit (Algeria)

10a) EPMA analyses (5 points along an yy' axis similar to that shown in figure 8) associated with data marked area II in table 7.

10b) EPMA analyses (5 points along an yy' axis similar to that shown in figure 8) associated with data marked area III in table 7.

EPMA and micro-PIXE data for Ga analysis within the sphalerites originating from Kipushi and Djebel Gustar respectively. For the high energy Ga Kα emission analysis using a 30 keV primary beam energy with the EPMA the C_{Ga}/K_{Ga} ratio is only ~ 1.08 and the error on the concentration is mainly the error due to statistical fluctuations of the measured intensities. However, the Ga concentrations derived from Ga Kα and Ga Lα measurements were consistent for both analyzed specimens.

As shown by equation [9], the value of the primary beam energy must be optimized taking into account the absorption effect of the measured X-ray photons by the matrix. The low energy Ga Lα emission exhibits a very strong absorption coefficient for the ZnS compound. For a 40° take-off angle of the WDS spectrometers used with the EPMA, a value Ep = 9.4 keV would correspond to the optimum peak/background ratio for the Ga Lα (λ= 11.29 Å or E = 1.096 keV) emission within the ZnS matrix. Other impurities such as Fe, Cu... were analyzed within the same specimen. The primary beam energy was increased up to 20 keV in order to keep the incident energy constant for all the analyzed elements.

Thus for the Ga Lα emission the 20 keV incident energy, Ep, leads to a high value of ~16 for the overvoltage, $U = Ep/E_L$ where E_L is the ionization energy of the Ga Lα level.

For high overvoltage values, the ZAF models may become inaccurate. We used another model designated PAP whose efficacy has been demonstrated for the case of high overvoltage and light element analysis [19].

The same experimental data for Ga within the sphalerite from the Kipushi deposit were processed by the use of the ZAF and PAP models. The Ga Kα (Ep = 30 keV) and Ga Lα (Ep = 20 keV) were measured.

For the Ga Kα occurring at 9.25 keV, i.e. an overvoltage ≃ 3, the percent difference is only ~ 1.5 % between the data derived from the ZAF and PAP models. As shown in table 8 below, the percent difference reaches ~5 % in the case of the Ga analysis by using the Ga Lα under experimental excitation leading to a high overvoltage value.

Thus the Ga concentration derived from Ga Kα and Ga Lα measurements with the EPMA were consistent and can be compared with micro-PIXE data.

Mercury : Micro-PIXE analyses showed that Hg was present with Ga and Cd in the specimen from Djebel Gustar. As shown in table 7 the Hg concentrations measured with the micro-PIXE vary from ~ 1900 ppm to ~ 2600 ppm depending on the location of the analyzed areas. As for Ga (figure 10 and table 7), two groups of Hg concentrations were obtained from EPMA measurements. For areas marked I and II in table 7, the Hg concentrations were the average of the measurements at the two closest locations of the area analyzed with the micro-PIXE. The five point measurements were averaged for areas III and IV respectively. The EPMA data for Hg are reported in table 7. However, while the Cd and Ga concentrations measured with micro-PIXE and EPMA were consistent, large discrepancies occurred for Hg. These variations more probably result as much from analytical problems as from the heterogeneity of the specimen.

Mercury was also detected by micro-PIXE in the specimen from the Saint-Veran deposit (Hautes-Alpes, France). Cd was also detected and, as reported in table 4, EPMA and micro-PIXE data for Cd were in good agreement. The EPMA also showed that Cu was present with an average concentration of ~ 1850 ppm. The effect of Cu, not detected with the micro-PIXE due to the Al absorber, was neglected in the Hg data calculation with the micro-PIXE.

As shown in table 9, the Hg concentrations derived from micro-PIXE data (Hg Lα at 9.98 keV) for the specimen from Saint-Veran ranges from ~ 560 ppm to 1200 ppm while Hg was not detected with EPMA using the Hg Mα (2.19 keV) emission. As previously reported, the limit of detection for a 3 σ criterion was ~1500 ppm for EPMA.

Hg analyses with EPMA were then performed using the Hg Lα emission as in the micro-PIXE analyses. For this purpose the primary beam energy was increased up to 30 keV and the counting time extended to 30 sec. A LiF monochromator was used. Again, the average net peak intensity was not statistically valid above the continuum intensity ; 40 % of the measurements indicated a positive but not significant value and 60 % of the measurements led to zero and negative values.

For a 3 σ statistical criterion the limit of detection should be 800 ppm.

Thus, neither Hg Mα nor Hg Lα analysis with the EPMA led to the detection of mercury within the sphalerite from Saint-Veran while the micro-PIXE indicated concentrations from ~560 to ~ 1200 ppm.

The same conclusions are drawn in the case of Hg analysis within the specimen from Djebel Gustar. Considering the Hg Mα emission, two of the four analyzed areas exhibited a statistically significant concentration (Table 7). Some experiments were carried out by using Hg Lα emission (30 keV primary beam energy). Ten measurements were performed at ten locations randomly distributed within the specimen. The average concentration was close to the statistical limit of detection for the experimental condition used (C_{MDL} = 800 ppm). The maximum Hg concentration was ~ 1500 ppm and the minimum observed concentration above the limit of detection was ~ 1000 ppm. Again, these results are consistent with those obtained by using the Hg Mα emission but none are consistent with micro-PIXE data. These are then significant discrepancies between the EPMA and micro-PIXE data for Hg, which may be due in part to the peak overlap between Zn Kβ and Hg Lα. The poor Hg detection limit in EPMA is surprising ; it may result from an overestimated intensity of the continuum but is probably due to the very low counting rate for the Hg Mα peak and the continuum measured with the PET monochromator, and also to the low peak to background ratio for the Hg Lα measured with the LiF monochromator. Another possible explanation for the low sensitivity of EPMA is the existence of beam damage, i.e. composition changes induced during electron irradiation. Such an effect has already been illustrated in the case of sphalerite specimens by studying the cathodoluminescence property changes as a function of electron bombardment time (20, 23) and in the case of Ag in chalcopyrite (21). Thermal and electrical effects which develop during electron irradiation may be sufficient to provoke ionic diffusion from the bulk to the surface or vice-versa.

Selenium : Micro-PIXE analyses showed that Se was present within the sphalerite from the Saint-Veran deposit. The presence of small amount of mercury which was also detected was neglected to process data characteristic of Se leading to a concentration of ~ 200 ppm (see table 9).

The specimen was analyzed with EPMA using a 20 keV primary beam energy and 30 sec. counting time with the background measured on each side of the Se L peak. Ten measurements were repeated and all of them were equivalent to an experimental concentration (uncorrected for the matrix effect) of ~ 130 ppm. However, considering a 3 σ criterion to obtain a significant characteristic peak above the continuum intensity, none of the measurements was valid. Taking account of the matrix effect for Se Lα by the ZnS composition the limit of detection was 570 ppm. Thus, Se is not detected with the EPMA, while the micro-PIXE indicated a Se concentration of 200 ppm (Table 9).

Table 7 - EPMA and micro-PIXE data of the sphalerite from the Djebel Gustar deposit (Algeria)

Area	Cu (ppm)	Cd (ppm)		Ga (ppm)		Hg (ppm)	
	EPMA	EPMA	micro-PIXE	EPMA	micro-PIXE	EPMA	micro PIXE
I	2350	2815 ± 225	2201 ± 78	1230 ± 800	1295 ± 375	n.d. to 1300	2490 ± 320
II	2515	2890 ± 225	2164 ± 79	n.d. to 3500	1510 ± 370	1480	1927 ± 325
III	2380	2270 ± 225	1852 ± 73	1500	1474 ± 375	n.d.	2091 ± 320
IV	2000	2356 ± 225	2632 ± 88	n.d.	388 ± 315	1600	2673 ± 236

n.d. : The peak to continuum intensity ratio is positive but none of the measurement satisfies the 3 σ criterion for statistical significance.

Table 8 - Comparison between Ga results derived from the same experimental data processed by means of the ZAF and PAP models successively.
Specimen : sphalerite from the Kipushi deposit (Zaire)

Ep keV	X-ray emission	Calculated Ga % weight concentration (average of 5 measurements) ZAF model	PAP model	Percent difference %
30	Ga Kα	2.15	2.12	1.4
20	Ga L α	2.77	2.90	4.7

Table 9 - EPMA and micro-PIXE analysis for Hg and Se in the sphalerite from the Saint-Veran deposit (Hautes-Alpes, France)

Hg (ppm)		Se (ppm)	
EPMA	micro-PIXE	EPMA	micro-PIXE
n.d.	564 ± 255	n.d.	209 ± 34
n.d.	1202 ± 309	n.d.	204 ± 32

Note - Cd was detected with EPMA and micro-PIXE (see table 4).
- Cu detected with the EPMA (~ 1850 ppm) was not detected with the micro-PIXE (Al absorber).
- n.d. : not detected.

Discussion

For Ag-bearing chalcopyrite, an excellent agreement between data was obtained by comparing successive EPMA and micro-PIXE analyses. Indium was detected with micro-PIXE but was not with EPMA.

For sphalerite specimens, EPMA and micro-PIXE data were in good agreement for Cd, Ag, Ge and Ga concentrations. The percent differences were within an acceptable level given the heterogeneity of the impurity distribution which would require a greater number of micro-PIXE analyses to perform more accurate comparisons.

Some discrepancies exist for Hg analysis with both techniques but the micro-PIXE was able to detect Se and In which were not detected with EPMA. Taking into account the large variations of the matrix composition (Fe and Cu), these comparisons support the analytical procedures used for intensity measurements and concentration calculations with both techniques, thus making possible the comparisons of calculated statistical limits of detection. In addition the comparisons between EPMA and micro-PIXE data are possible since we verified by calculations of X-ray yields that the accuracy of measurements is less influenced by surface contamination for the case of micro-PIXE than for EPMA.

It has been shown that the existence of thin surface films containing an element assumed to be homogeneously distributed within the volume may affect the reliability of EPMA analysis (21). Contamination by Ag has been reported at the surface of sulfide minerals in contact with silver bearing sulfide (21) or containing Ag as volume impurity. Theoretical calculations of PIXE yields (6) show that an X-ray intensity equivalent to ~300 ppm Ag in the volume of ZnS corresponds also to a Ag surface film of ~ 5 nm thickness. For a ~ 5 nm pure Ag film on top of ZnS, the apparent measured concentration with the EPMA would decrease from ~ 2 % down to 0.8 % when increasing the primary beam energy from 15 to 30 keV respectively. Therefore, if surface contamination by the element of interest occurs, the micro-PIXE data will be only slightly affected by the surface film and this effect will be neglected in calculating the MDL.

As shown in table 10 the C_{MDL} with the micro-PIXE for a ZnS matrix is superior by a factor ~10 to ~ 30 as compared to the C_{MDL} with the EPMA for the analysis of Se, Ag, Cd and In.

For Ga, Ge and Hg, the C_{MDL} with the micro-PIXE is only better by a factor of ~ 3 as compared to the EPMA data when the low energy X-ray emissions Lα and Mα respectively are used and by a factor of ~ 2 when the Kα and Lα X-ray lines are used. The lower sensitivity of the micro-PIXE for Ga, Ge and Hg as compared to the sensitivity for Se, Ag, Cd, In, results from differences in the attenuation of the X-ray intensities by the Al absorber placed in front of the detector. As an example, with a 750 μm thick Al absorber used for ZnS analysis, transmission factors for Ga, Ge and Hg Lα are 0.00159, 0.00497 and 0.00589. For the Kα lines of Se, Ag, Cd, In, they are 0.0256, 0.612, 0.650 and 0.674.

In the future, efforts in micro-PIXE instrumentation development should concern the choice of the nature and thickness of absorbers to optimize the transmission efficiency for various matrices. Such optimization is required to extend the domain of atomic number detectable in order to process spectra without having to rely on EPMA data as done in the present study.

Reducing the thickness of the absorber would lead to an increase of sensitivity for some elements. Assuming that the response of the detector would remain linear when a 350 μm thick Al absorber is used for ZnS analysis, the limit of detection for Cd, Ag and In should be improved by a factor of 1.25 as compared to the C_{MDL} (~ 15 ppm) which was obtained with the 750 μm thick Al absorber. However, for the elements Ga, Ge and Hg, the gain should be very large. For a 350 μm thick Al absorber the C_{MDL} for Ga, Ge and Ge should be 5, 10 and 30 ppm as compared to the 155, 185 and 470 ppm respectively obtained in the present study (Table 10). To prevent artifacts resulting from the high counting rate when the thickness of the absorber is reduced, beam switching technique could be used to improve the performance of the pulse processing unit of the spectrometer (13) (24).

The present micro-PIXE data, when large matrix effects are encountered, demonstrated the credibility of the fundamental parameters in the data base used for both intensity measurements and concentration calculations. The efficiency of the procedures used are particularly well emphasized by the analysis of Ga within the sphalerites. The situation for Ga analysis is complex, due to either the overlap occurring between the Ga Kα and Zn Kα peaks or the presence of Cu which is not detected with the micro-PIXE but plays an important role in the least-squares fitting procedure and X-ray yield calculation. An iterative procedure should be added to the actual least-square fitting analysis of the spectrum to derive intensities even in the case of minor elements which are not detected due to the Al absorber. This limitation may be avoided when using more appropriate filters or by combining both WDS and EDS for the micro-PIXE.

The limits of detection which were obtained with the EPMA for the experimental conditions described above may be also improved. One route is optimization of the primary beam energy leading to higher peak to continuum intensity ratio for the analyzed element within a given matrix ; this approach is only valid for analysis on a routine basis if automatic beam focusing for each condition used is available with the EPMA. Another option is to use digital recording of spectra (step by step monochromator displacement for data acquisition) which then permits use of least squares fitting techniques (as used with the EDS in EPMA and micro-PIXE analysis). An improvement of the model used for continuum removal may be preferable to the use of blank specimens in view of variable impurity content. Increase of the counting time in order to get a better statistical precision for both the peak and the continuum intensity is an obivous option. As an example, the calculate minimum detection limit for Hg (20 keV, Hg Mα) decreased from 1180 ppm to 850 ppm, 725 ppm and 270 ppm successively when the counting time was increased from 30 sec. to, 60, 120 and 600 sec. respectively. However the possibility of specimen damage by increased irradiation dose has to be set against the MDL improvement.

Table 10 - Calculated statistical limit of detection for a ZnS matrix with EPMA and micro-PIXE under the specific measuring conditions pertaining to this work (see experimental section).

Element	micro-PIXE*		EPMA**	
	X-ray emission	3 σ limit of detection (ppm)	X-ray emission	3 σ limit of detection (ppm)
Fe	Not detected due		Kα	250
Cu	to Al absorber		Kα	320
Ga	Kα	155	Lα Kα	840 230
Ge	Kα	185	Lα	120
Se	Kα	53	Lα	570
Ag	Kα	13	Lα	380
Cd	Kα	15	Lα	395
In	Kα	16	Lα	500
Hg	Lα	470	Mα Lα	1400 800

micro-PIXE : 4 MeV proton energy, Al absorber in front of the detector, acquisition time corresponding to 250,000 measured Rutherford counts.

EPMA : 30 second counting time, 20 keV primary beam energy except for Ga Kα and Hg Lα (30 keV).

Summary

EPMA and micro-PIXE complementarity for minor and trace element localization in sulfides has been evaluated. Chalcopyrite and sphalerite from various deposits have been analyzed with emphasis on Ag, Cd, In, Se, Ga, Ge and Hg. Reproducibility, statistical precision and accuracy were discussed.

For Ag-bearing chalcopyrites, excellent agreement between data was obtained by comparing successively EPMA analyses carried out by different laboratories and micro-PIXE data from two independent analytical runs. For micro-PIXE, the statistical detection limit is improved by a factor of ~ 10 as compared to the EPMA limit (300 ppm for the experimental conditions used).

Micro-PIXE analyses of (Zn,Fe)S matrices are much more complex than for chalcopyrite because of large variations in composition from a specimen to another as well as within a specimen exhibiting heterogeneity at the microscopic scale. This large composition variations made difficult the comparisons between EPMA and micro-PIXE data. This study emphasized the problems encountered in trace element analysis with both techniques. Depending upon the energy of the analyzed X-ray photons, the X-ray intensities and X-ray yields may be more or less influenced by Fe concentration variations and to a lesser extent, by the presence of other impurities such as Cu, Ga... We used concentration data derived from EPMA analyses of the major and minor constituents to process the micro-PIXE data characteristic of the trace elements of interest.

Experimental and calculated data showed that Cd Kα, Ag Kα, In Kα Hg Lα X-ray emissions may be processed by using an average composition of the (Zn,Fe)S matrix whereas data manipulation for Ge Kα and more particularly Ga Kα required an accurate knowledge of the matrix composition.

For Cd analysis with concentrations ranging from ≃ 1000 to 7000 ppm, the difference between EPMA and micro-PIXE was ≃25 %. A difference of about 25 % was also obtained in the case of Ga (0.1 to 1.3 %) with Cu concentrations ranging from 0.2 to 2 % and thus creating a large matrix effect for the Ga Kα X-ray emission.

The comparison of EPMA and micro-PIXE data demonstrated the credibility of the models used for data processing with the micro-PIXE and the validity of both techniques for quantitative analysis of a few hundreds to thousands of ppm.

Some trace elements such as In, Se, Hg were detected by means of the micro-PIXE but were not detected by EPMA analysis. However, owing to instrumental factors, some minor elements (Fe, Cu) in the sphalerite specimens were not analyzed by the use of the micro-PIXE. The comparisons demonstrated the complementarity of EPMA and micro-PIXE for studying the localization of trace elements in sulfide minerals.

Acknowledgements

The authors thank C. Gilles and G. Vard for their contribution to the EPMA analyses, G. Clavel and C. Remond for their contribution in data acquisition by means of micro-PIXE and W.J. Teesdale for help in data analysis. Thanks are also due to F. Boyer, University Pierre et Marie Curie, Paris, for providing most of the specimens used in this study.

References

(1) Barbi NC, Skinner DP, Molensky VS (1980) A minimum standards technique for semi-quantitative energy dispersive X-ray microanalysis. 8th International Conference on X-ray Optics and Microanalysis ; DR Beaman, RE Ogilvie, DB Wittry (eds) Pendell Publishing Co, Midland, U.S.A., 133-135.

(2) Blank H, Traxel K (1984) Proton induced X-ray emission in micro regions applied in mineralogy. Scanning Electron Microsc. 1984 ; III : 1089-1096.

(3) Bosch F, El Goresy A, Herth W, Martin B, Nobiling R, Povh G, Reiss HD, Traxel K (1980) The Heidelberg proton microprobe, Nuclear Science Applications, 1, 33-55.

(4) Cabri LJ, Blank H, El Goresy A, Laflamme JHG, Nobiling R, Sizgoric MB, Traxel K (1984) Quantitative trace-element analyses of sulfides from Sudbury and Stillwater by proton microprobe. Canadian Mineralogist, 22, 521-542.

(5) Cabri LJ, Campbell JL, Laflamme JHG, Leigh RG, Maxwell JA, Scott JD (1985) Proton microprobe analysis of trace elements in sulfides from some massive-sulfide deposits. Canadian Mineralogist, 23, 133-148.

(6) Campbell JL, Cookson JA (1984) PIXE analysis of thick targets. Nuclear Instruments and Methods in Physics Research, B 3, 185-187.

(7) Campbell JL, Cookson JA, Paul H (1983) Uncertainties in thick target PIXE analysis. Nuclear Instruments Methods, 212, 427-439.

(8) Campbell JL, Maenhaut W, Bombelka E, Clayton E, Malmqvist K, Maxwell JA, Pallon J, Vandenhaute J (1986) An intercomparison of spectral data processing techniques in PIXE. Nuclear Instruments and Methods in Physics Research, B 14, 204-220.

(9) Campbell JL, Millman BM, Maxwell JA, Perujo A, Teesdale WJ (1985) Analytical fitting of monoenergetic peaks from Si(Li) X-ray spectrometers. Nuclear Instruments and Methods in Physics Research, B 9, 71-79.

(10) Giraud R, Remond G, Pajon D, Henoc J, Conty C, Tong M (1979) Automated WDS qualitative and quantitative microanalysis in geosciences. In Microbeam Analysis, DE Newbury (eds) San Francisco Press, 91-100.

(11) Harris DC, Cabri LJ, Nobiling R (1984) Silver bearing chalcopyrite, a principal source of silver in the Izok massive-sulfide deposit : confirmation by electron and proton microprobe analyses. Canadian Mineralogist, 22, 493-498.

(12) Henoc J, Heinrich KFJ, Myklebust RL (1983) A rigourous correction procedure for quantitative electron probe microanalysis (COR 2). NBS Technical Note 769, 1-132.

(13) Koenig W, Richter FW, Steiner J, Stock R, Thielmann R, Watjen U (1977) Trace element analysis by means of particle induced X-ray

emission with triggered beam pulsing. Nuclear Instruments and Methods, April 1-15, 142, n° 1, 2, 225-229.

(14) Kyser DF (1972) Experimental determination of mass absorption coefficient for soft X-rays. 6th International Conference on X-ray Optics and Microanalysis, G. Shinoda, K Kohra, T. Ichinokawa (eds) University of Tokyo Press, 147-156.

(15) McCarthy JJ, Schamber FH (1981) Least squares fit with digital filter : a status report. In: Energy Dispersive X-ray Spectrometry, KFJ Heinrich, DE Newbury, RL Myklebust, CE Fiori, (eds) NBS Special publication 604, 273-296.

(16) Maxwell JA, Leight RG, Campbell JL, Paul H (1984) Least-squares fitting of PIXE spectra with a digital filter treatment of the continuum. Nuclear Instruments and Methods in Physics Research, B 3, 301-304.

(17) Myklebust RL, Fiori CE, Heinrich KFJ (1981) Spectral processing techniques in a quantitative energy dispersive X-ray micro-analysis procedure (Frame C). In : Energy Dispersive X-ray Spectrometry ; KFJ Heinrich, DE Newbury, RL Myklebust, CE Fiori, (eds). NBS Special Publication 604, 365-380.

(18) Philibert J, Bryckaert D, Tixier R (1972) Invariability of intensity ratios for standards. 6th International Conference on X-ray Optics and Microanalysis. G. Shinoda, K. Kohra, T. Ichinokawa (eds). University of Tokyo Press, 157-162.

(19) Pouchou JL, Pichoir F (1984) Un nouveau modèle de calcul pour la microanalyse quantitative par spectrométrie de rayons X. Partie I : Application à l'analyse d'échantillons homogènes. La Recherche Aérospatiale, n° 3, 167-192.

(20) Remond G (1977) Applications of cathodoluminescence in mineralogy. J. of Luminescence, 15, 121-155.

(21) Remond G, Giraud R, Packwood RH (1984) The effect of volume and surface diffusion of impurities on the detection limit in microprobe analysis. Scanning Electron Microsc. 1984 ; I : 151-166.

(22) Remond G, Joseph E, Jeanrot P (1972) Evaluation de la correction d'absorption dans l'analyse quantitative des silicates. 6th International Conference on X-ray Optics and Microanalysis ; G. Shinoda, K Kohra, T. Ichinokawa (eds) University of Tokyo Press, 203-209.

(23) Remond G, Le Gressus C, Okuzumi H (1979) Electron beam effects observed in cathodoluminescence and Auger electron spectroscopy in natural materials : evidence for ionic diffusion. Scanning Electron Microsc. 1979 ; I : 237-244.

(24) Statham P (1981) Electronic techniques for pulse processing with solid-state X-ray detector. In : Energy Dispersive X-ray Spectrometry ; KFJ Heinrich, DE Newbury, RL Myklebust, CE (Fiori (eds) NBS Special Publication 604, 141-164.

Discussion with Reviewers

Reviewer I : I assume that sphalerite and chalcopyrite are stable under proton bombardment in the said analytical conditions. However, silver-, mercury-, or selenium-rich sulphide minerals usually decompose under such an analytical condition (4 MeV, 20-minute bombardment) and the bulk composition of the analyzed area usually changes during the counting period unless special cares have been taken to prevent the decomposition. Had this type of phase decomposition been encountered during your trace analyses of Ag, Hg and Se by micro-PIXE ?

J. Minkin : The concentration determinations for Hg seem consistently lower with EPMA than with micro-PIXE. Doesn't this therefore give a strong indication that in the case of EPMA the electron irradiation with its shallow penetration is probably causing much local heating and consequent volatilization of the Hg, compared to the much-reduced effect of this nature which PIXE would have with its much greater penetration and therefore less localized heating ?

H. Blank : You expect the low sensitivity of EPMA for Hg being due to composition changes induced during electron irradiation. Could you also find composition changes being due to proton beam damage ?

Authors : All questions above emphasize two major points which may affect the reliability of data obtained by means of EPMA and micro-PIXE respectively i.e. : what is the irradiation dose required to induce beam damage during electron or proton bombardment? and how sensitive are both techniques to detect the beam damages induced during the energy loss process for the incident electrons and protons interacting with the solid respectively ?

Beam damages i.e. composition changes during electron or proton bombardment result from several complex mechanisms such as stimulated desorption of species, thermal and or electrical enhanced diffusion. It is however difficult to predict which mechanism will be predominant since for a given incident energy, the effects will depend upon the element, the crystallographic structure, the existence of defects.

For a particular material, the creation of damages and their kinetics will depend simultaneously upon both the penetration depth of the incident particles (dimension of the analyzed volumes) and upon the distribution depth of the energy losses during inelastic scattering processes (shape of the analyzed volume). 4 MeV protons will penetrate much more deeper than ~20 keV electrons. As an example, for a ZnS substrate the penetration depth of electrons with ≃ 20 keV incident energy is only of few microns while this depth can reach ~100 µm when 4 MeV protons irradiate the target.

In addition, under electron irradiation, the energy dissipation per unit of depth exhibits a maximum near the surface indicating that a high fraction of the incident energy is lost at a low depth as compared to the total range of electron penetration. Combining

surface sensitive techniques and the EPMA, Remond et al. (Scanning Electron Microsc., 1982 ; III : 995-1011 and Scanning Electron Microsc., 1984 ; I : 151-166) showed that electron beam irradiation may induce surface lateral diffusion and/or segregation of impurities from the bulk to the surface or vice-versa. The sensitivity of the method to detect the surface or sub-surface composition changes will depend upon the ionization distribution function and the escape depth of the generated photons within the volume. These authors also showed that due to the ionization distribution function with depth, the EPMA is very sensitive to detect very thin surface films bearing the elements assumed to be homogeneously distributed within the volume. In the case of proton irradiation Dyson and Fakhouri (X-ray Spectrometry, 1986, 15, 201-205) recently claimed that the ionization depth distribution resulting from scattering of protons also exhibited a maximum near the surface, a result which has not yet been confirmed by others.

However, since the Rutherford backscatter cross section is small, and since protons are scattered through angles which are much smaller than for electrons, the existence of a maximum in the energy loss function versus depth more probably results from some other mechanisms (as yet not incorporated in standard PIXE theory) rather than from excitations by protons scattered towards the surface. Thus, although there is no direct evidence for beam damage induced by protons by combining surface sensitive techniques and micro-PIXE, such effect may occur.

Therefore, for concentrations ranging from a few hundreds to a few thousands ppm as considered in the present study, small surface composition changes will not be detectable with the micro-PIXE. For this reason, if beam damages occur for Hg during proton bombardment this effect will be probably much smaller than for electron bombardment and will not be detected by micro-PIXE. No evidence for beam damage was shown for Se either with proton or electron irradiation. In addition, Cabri et al. (see ref. 4 in text) studying trace elements in pentlandite minerals showed that an excellent agreement between data resulting from EPMA analysis of areas which were previously exposed to proton irradiation. These observations tend to confirm that if proton induced damage exists, it is too small to be detected.

J. Minkin : What do you use as the demarcation between minor and trace -element concentrations ?

Authors : The limit between minor and trace elements is a subjective notion and may be arbitrarly defined. It is generally accepted from a mineralogical point of view to define trace elements, as those being present with concentration in the order of magnitude of several hundreds of ppm or less while minor elements have concentrations ranging from one to a few percent. It is obvious that such limits may change as a function of the analytical methods used.

J. Minkin : The impressive general agreement of the data of Harris et al. (1984) for Ag from Izok Lake with your data strongly emphasizes the accuracy of your "standardless" data quantification procedures, as I believe Harris et al. reduced their data against natural and synthetic standards. However, the Ag data of Harris et al. for the Hilton Mine samples appear to be consistently higher than yours - do you attribute this to a sampling problem ? Did you analyze any areas on their original samples ?

Authors : Harris et al. (Canadian Mineralogist, 1984, 22, 493-498) analyzed the same areas of chalcopyrite specimens from Hilton Mine and Izok Lake deposits by means of EPMA and micro-PIXE. Comparisons showed excellent agreement between data obtained by using different synthetic materials containing Ag in small amounts as reference compounds. Three specimens from Hilton Mine were analyzed leading to Ag concentrations of ~1700 ppm, ~2300 ppm and ~3000 ppm depending upon the analyzed specimen. The differences observed with our present data probably result from the heterogeneity of the specimens since the specimen analyzed in the present study are not those studied by Harris et al. In addition EPMA analyses reported by Harris et al. were not corrected for matrix effect.

J. Minkin : With respect to EPMA quantitative analysis based on standards, do you think that if instead of pure elements, standards are used which have lower concentrations of elements of interest in a matrix similar to that of the unknown (assuming such samples can be found in nature or synthesized with adequate homogeneity), would this result in better data, i.e. smaller s.d.'s and lower MDL's ?

Authors : The use of pure element or compounds containing high concentrations of the element of interest leads to a high counting rate allowing to set accurately the monochromator to the Bragg's position. However, the peak intensity measurement must be carefully corrected for possible loss of data resulting from high dead time and from shift of the pulse height distribution in the PHA. The use of compounds as reference materials with composition close to that of the unknown will lead to intensity measurements having the same statistical precision. However increasing the precision will not change the matrix effect. The improvement in the limit of detection lies essentially in a more accurate measurement of the intensity of the continuous emission under the characteristic peak. The use of "blank" specimens is a possible approach to this problem. However, fitting or digital filtering procedures will provide a more general approach when a large number of compounds containing many trace elements has to be analyzed.

E.T. Williams : What is the total time required for a complete EPMA analysis (i.e. : such as that for Table 1) compared to the 20 minutes cited for one PIXE analysis ? Why do you make 10 measurements of a sample by EPMA versus 1 for PIXE ?

Authors : Four monochromators can be used simultaneously either for qualitative and quantitative data acquisition. Thus for a qualitative analysis (see Fig. 1) the monochromators are moved step by step and the full range of analyzed wavelengths is explored in about 5 minutes. The equipment is under the control of a microprocessor unit (data acquisition) and a computer (data handling). By the use of the microprocessor each of the four spectrometers acts virtually as if it has its own automation unit (asynchronous displacement of each monochromator). Thus, this

situation allows one to select different counting times for the elements to be analyzed within the same run.

Therefore, the total acquisition time is imposed by the longest total counting time of operation for a given spectrometer. For the case of Ag analysis in $CuFeS_2$ the total time including both the data acquisition for the major and trace elements and the data reduction is in the order of magnitude of 120 sec.

E.T. Williams : How does the penetration depth of the electrons (15-30 keV) compare with that of 4 MeV protons ?

Authors : The mean atomic number for a $CuFeS_2$ matrix is Z = 23.5. In a first approximation we can assume that the penetration depth for electron 15-30 keV energy will remain in the same order of magnitude than that for electrons penetrating a pure Cu target. Depth distribution for electrons, backscattered electrons and X-ray photons has been extensively studied either experimentally ("sandwich" technique) or theoretically by the use of Monte Carlo calculation or by the use of the Boltzman transport equation. As illustrated by DE Newbury and H. Yakowitz the total penetration depth of electrons into copper increases from 0.2 to ~1 μm when the energy is increased from 10 to 20 keV, the incident beam being normal to the surface of the specimen (DE Newbury, H. Yakowitz, (1976), use of Monte Carlo calculations in electron probe microanalysis and scanning electron microscopy, KFJ Heinrich, DE Newbury, H. Yakowitz (eds), NBS special publication 460, 15-44). Obviously, Cu Kα photons are generated from smaller depth than the total depth of penetration of the electrons since their energy must be greater than the ionization energy of the Cu K level. In addition the analyzed depth must take into account the escape depth of the generated photons interacting with the matter. Therefore for the experimental conditions used in the present study an average analyzed depth may be estimated to be ~ 1 μm.

With the 4 MeV proton beam energy the total penetration depth is much greater than for electron irradiation. As an example figure 11 illustrates the variation with depth of the percent number of photons relative to the total number of Ag Kα photons measured at the surface of a ZnS substrate containing 0.1 wt % of silver (similar results should be obtained for the case of a chalcopyrite specimen containing 0.1 wt % of silver as bulk impurity).

For the above calculation the 4000 keV incident proton energy was divided into 40 steps of equal energy loss as a function of depth. The number of photons generated within a thin "slice" of thickness, z, below the surface was calculated for each of the 40 steps. The number of emitted photons was then calculated taking account for the attenuation by the matrix of the number of generated photons as a function of depth. For the ZnS (or $CuFeS_2$) matrix, the total penetration depth of protons was in the order of magnitude of ~ 100 μm. The escape depth for the Ag Kα photons was ~ 60 μm when 95 % of the total number of photons are produced.

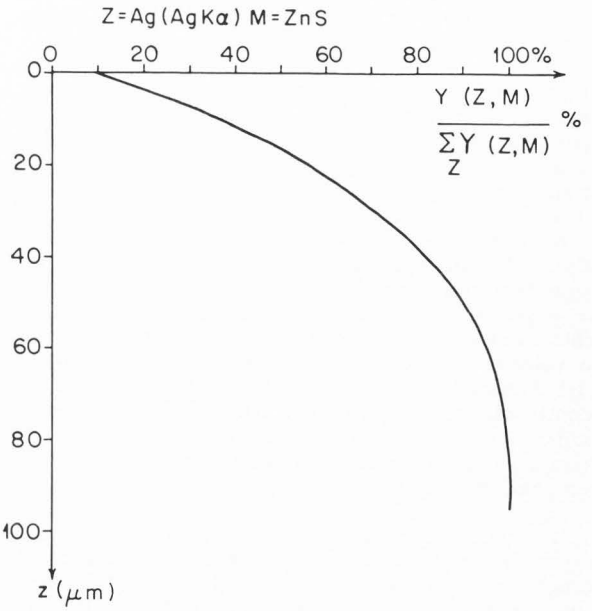

Figure 11 - Number of Ag Kα measured photons (0.1 wt % Ag in ZnS) with respect to the total Ag Kα yield as a function of the penetration depth of 4 MeV protons.

E.T. Williams : What were the diameters of the proton and electron beams used in the analysis ?

Authors : In practice, it is usual with the EPMA to evaluate the electron beam diameter from observing either the luminescence emission or the contamination spot which often develop during beam irradiation. Specimens such as cassiterite, SnO_2, or thorite SiO_4Th emit cathodoluminescence and are often used to control the beam alignment and beam diameter. In the present study some of the sphalerite specimens emitted luminescence under electron and proton irradiation and were used to locate the position of the beams. The luminous photons generated within the volume interact with the solid before to merge at the surface of the specimen. The diameter of the luminescent spot observed at the surface of the specimen is greater than the diameter of the electron or proton beam resulting from scattering effect.

As illustrated in Fig. 8, beam diameter can also be evaluated from the size of the contamination spots which develop at the surface of the specimens. For a given specimen, the lateral size of the damaged area depends on the total irradiation dose and may change as a function of time resulting from various mechanisms such as stimulated adsorption or desorption and lateral diffusion of some species.

Thus observation of both cathodoluminescence and contamination spots leads to an overestimated evaluation of the diameter of the incident beam. In the present study, the electron beam diameter was estimated to be < 2 μm and the proton beam size to be ~ 4 μm x 6 μm in size.

H. Blank : Chen et al. [NIM B3, (1984), 241-245] report comparison of PIXE and synchrotron radiation analysis. Do you intend to apply synchrotron radiation analysis on your samples ?

Authors : The major advantage of proton and synchrotron irradiation over electron bombardment is to induce a low intensity of the continuous X-ray emission. However, X-ray spectrometry using synchrotron irradiation and micro-PIXE complement the electron probe microanalysis taking account for the easy use of EPMA equipment for analytical problems requiring a large number of point analyses. Owing to the chemical heterogeneity of minerals, the techniques to be used for trace element localization must provide high lateral resolution. Thus our future work will aim to compare X-ray spectrometry with secondary ion mass spectroscopy induced either by ion bombardment or laser irradiation applied to trace and infratrace element analyses.